Clays and Clay Minerals, Vol. 59, No. 5, 446–458, 2011.

ENHANCED FLAME-RETARDANT CAPACITY OF NATURAL RUBBER/ORGANO-MONTMORILLONITE AND HYPER-BRANCHED ORGANO-MONTMORILLONITE COMPOSITES

JINCHENG WANG*, XI GUO, XIAOYU ZHENG, YI ZHAO, AND WEIFEI LI

College of Chemistry and Chemical Engineering, Shanghai University of Engineering Science, Shanghai 201620, P.R. China

Abstract—Most natural and synthetic rubbers have inherently high flammability, a property which limits their uses. The aim of the present work was to study the effect of organo-montmorillonite (OMMT) and modified OMMT on the flame-retardance and mechanical properties of natural rubber (NR) composites. The OMMT was modified with hyper-branched polymer *via* condensation polymerization between the intercalation agent, N,N-di(2-hydroxyethyl)-N-dodecyl-N-methylammonium chloride, and the monomer, N,N-dihydroxyl-3-aminomethyl propionate. This modified OMMT was then reacted with phosphate, and a novel flame-retardant hyper-branched organic montmorillonite (FR-HOMMT) was thus obtained. The surface morphology, interlayer space, interlamellar structure, and thermal properties of these modified clays were investigated by Fourier-transform infrared spectroscopy, scanning electron microscopy, X-ray diffraction, and thermogravimetric analysis. The FR-HOMMT showed increased basal spacing and better thermal stabilities due to the different arrangement and thermal stability of the novel organic macromolecular surfactant. Natural rubber NR/OMMT and NR/FR-HOMMT composites were prepared by conventional compounding with OMMT and the phosphorus-based organo-montmorillonite. The cure characteristics, tensile strength, wear resistance, thermal stabilities, and flame-retardant properties were researched and compared. The best dispersion of this modified clay was observed for 20 phr (parts per hundred of rubber) of FR-HOMMT-filled composite, which resulted in the best mechanical performance with an increase of 47% in tensile strength, of 40% in elongation at break, and decrease of 140% in abrasion loss compared with 20 phr of the OMMT-filled matrix. A mechanism for reinforcing and flame retardance is proposed here. The 'anchor' effect caused by the hyper-branched polymer may decrease the number and size of the voids in the NR matrix, and thus increase the crack path during tensile drawing. Meanwhile, the flame retardance of the OMMT and the phosphate may increase the number of carbonaceous layers, thus inhibiting the degree of pyrolysis of the NR matrix during burning.

Key Words—Characterization, Flame-retardant, Hyper-branched Polymer, Montmorillonte, Natural Rubber.

INTRODUCTION

Natural rubber is composed mainly of polymerized *cis*-1,4-polyisoprene, and can be obtained from an aqueous dispersion from the rubber tree and as a dried solid phase (Powell and Beall, 2007). Compared with synthetic rubbers, NR is a material that has shown its worth both as a 'commodity polymer' and as an 'engineering elastomer' by virtue of its unique combination of physico-mechanical properties. One of the setbacks of most natural and synthetic rubbers that limits their uses in highly demanding applications is their inherently high flammability (Menon, 1997).

The use of flame-retardant additives allows the fire properties of the rubber composites to be minimized (Ismail *et al*., 2008; Wang and Chen, 2007). Montmorillonite has received special attention in the field of flame retardancy because of its high thermal stability, sub-microparticle size, and intercalation properties. Nanocomposites containing intercalated montmorillonite particles exhibit improved moduli, decreased gas permeability, and enhanced thermal stability (Gu *et al*., 2010; Wang *et al*., 2006; Zhou *et al*., 2002).

Exfoliation and dispersion of hydrophilic montmorillonite in a hydrophobic polymer matrix, however, is difficult. The flame retardancy of montmorillonite is sufficient for application in flammable polymers.

Three main objectives for modification of montmorillonite are: (1) to expand the interlayer space of the clay, allowing large polymer molecules to enter into the space; (2) to improve the miscibility of clay with the polymer, thereby achieving good dispersion of clays in the polymer matrix; and (3) to introduce a flame-retardant element into the clay, thereby improving the thermal stability of the organo-montmorillonite. Extensive studies of clay modification, especially by various organic surfactants, have been carried out (Aouad *et al.*, 2010; Monasterio *et al.*, 2010; He *et al.*, 2005; Lee *et al.*, 2005; Hedley *et al.*, 2007; Calderon *et al.*, 2008; Wang *et al.*, 2009a). Most of the investigations emphasized the importance of the interlayer space of the clays; the exfoliation could be controlled by controlling the arrangement of the surfactant molecules in interlayer

* E-mail address of corresponding author:
wjc406@263.net
DOI: 10.1346/CCMN.2011.0590502

space, *i.e.* in terms of chain length, charge density, and amount adsorbed (Zhao *et al.*, 2010; Boo *et al.*, 2006; Xu *et al.*, 2006). In the case of most linear organic surfactants, large basal spacings are normally achieved by addition of excess small-molar-mass organic surfactants, which will reduce significantly the thermal stability of the organo-clay, and could adversely affect flame-retardance properties of the clay, resulting in reduced flame-retardant behavior of the polymeric matrix.

A new class of macromolecules – hyper-branched polymers – has recently received attention because of special features, including porous and three-dimensional networks and numerous functional end groups; hyper-branched polymers are difficult to crystallize and are highly compatible with other polymers (Tan and Luo, 2005; Marlene *et al.*, 2004).

The hyper-branched polymer containing phosphorus behaves like a surfactant in surface modification. The flame-retardant effect of P and Si in montmorillonite and hyper-branched polymer can lead to new types of enhanced polymer composites.

The present study was undertaken to test the application of montmorillonite to NR using OMMT and a newly synthesized flame-retardant hyper-branched organo-montmorillonite, FR-HOMMT, as reinforcing and flame-retardant agents, respectively. A hyper-branched polymer was anchored to the inner surface of the clay nanoplatelets by condensation polymerization between –OH end groups in OMMT and the monomer which had been synthesized. The FR-HOMMT was analyzed using Fourier-transform infrared (FTIR) spectroscopy, scanning electron microscopy (SEM), X-ray diffraction (XRD), and thermogravimetric analysis (TGA). Then, the OMMT and HOMMT obtained were incorporated into a NR system. The properties of the NR/OMMT and NR/FR-HOMMT composites, such as cure characteristics (scorch time t_{10} and optimum cure time t_{90}), tensile strength, elongation-at-break, thermal stability, and flame-retardance properties were researched and compared.

EXPERIMENTAL

Materials

The organo-montmorillonite, marketed as OMMT, was supplied by Zhejiang Fenghong Clay Company (Zhejiang, China). The structural formula of the inorganic MMT is $Na_{0.71}Ca_{0.06}Mg_{0.014}(Si_{7.80}Al_{0.20})(Al_{3.14}Fe^{3+}_{0.20}Fe^{2+}_{0.04}Mg_{0.62})O_{20}(OH)_4$, and its cation exchange capacity (CEC) is 90 cmol/kg. The formula indicates that the negative layer charge arises largely from isomorphous substitution of Mg^{2+} for Al^{3+} in the octahedral sheet with some contribution from substitution of Al^{3+} for Si^{4+} in the tetrahedral sheet. The layer charge in MMT is mainly balanced by Na^+ ions occupying interlayer sites. To obtain OMMT, this MMT was modified with the intercalation agent, N,N-di(2-hydroxyethyl)-N-dodecyl-N-methylammonium chloride, the chemical formula of which is:

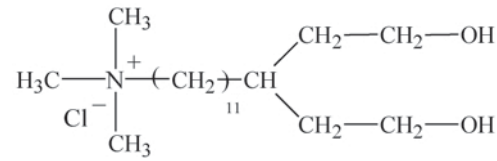

Synthesis of monomer

The materials tested in this study were synthesized in multiple steps (Figure 1). In the first step, a monomeric solvent was synthesized by combining 0.1 mol of diethanolamine (purity 98%, reagent grade, Shanghai Guoyao Chemical Company), 0.1 mol of methyl acrylate (purity 98%, reagent grade, Shanghai Guoyao Chemical Company), and 10 mL of methanol (purity 99%, reagent

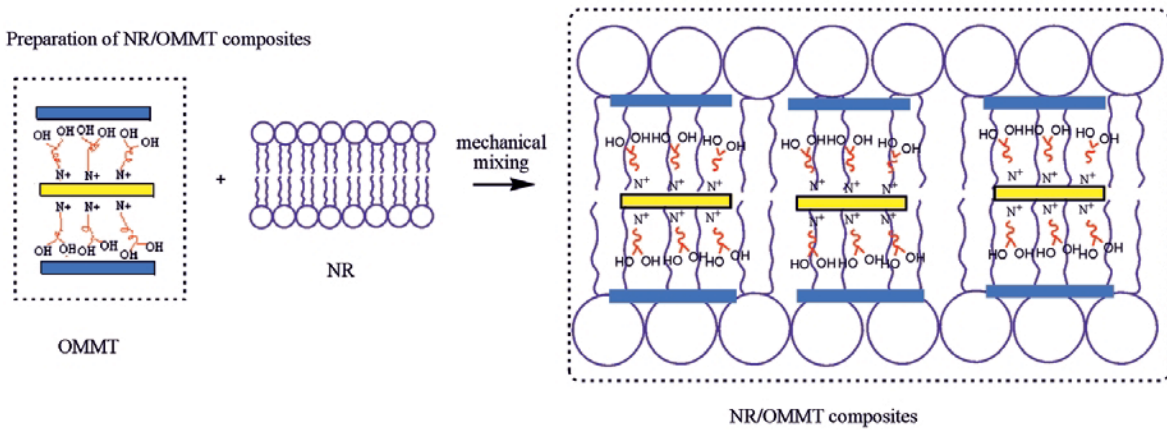

Figure 1 (*this and facing page*). Preparation steps and schematic diagrams of synthetic (a) NR/OMMT composites, and (b) NR/FR-HOMMT composites.

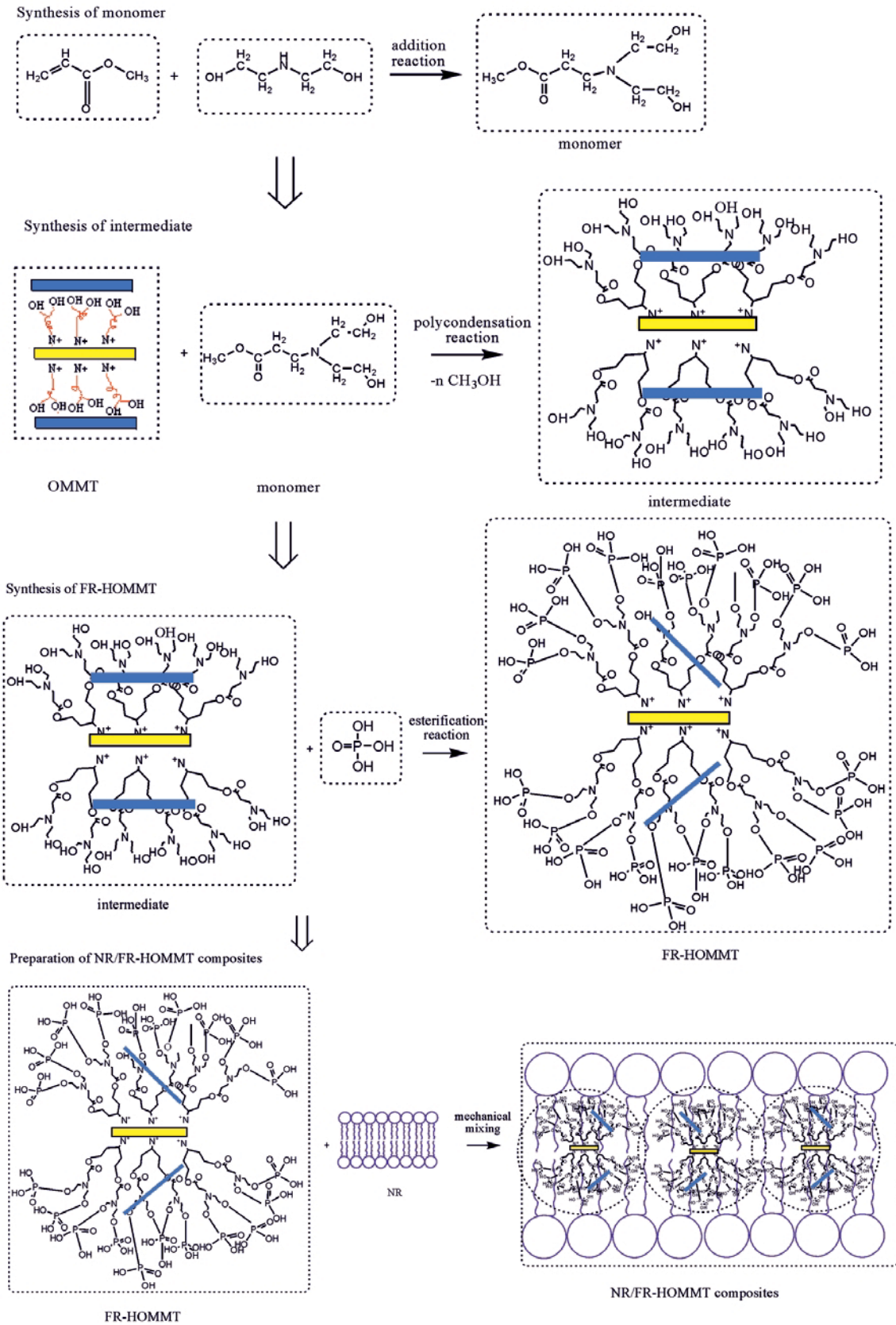
Synthesis of monomer
addition reaction
monomer
Synthesis of intermediate
polycondensation reaction
-n CH3OH
OMMT
monomer
intermediate
Synthesis of FR-HOMMT
esterification reaction
intermediate
FR-HOMMT
Preparation of NR/FR-HOMMT composites
mechanical mixing
NR
FR-HOMMT
NR/FR-HOMMT composites

grade, Shanghai Guoyao Chemical Company) in a three-necked flask provided with a stirrer. The mixtures were treated at 35ºC for ~4 h under an N_2 atmosphere. The product was separated using a separatory funnel method, and distilled until no methanol remained. The product, N,N-dihydroxyl-3-aminomethyl propionate, was obtained as a stable, transparent oily liquid and the yield was ~85% and was used as the solvent in the synthesis of the FR-HOMMT.

Synthesis of FR-HOMMT

In the second step (Figure 1), a 250 mL, four-necked flask with a mechanical stirrer, thermometer, and a tube supplying an N_2 atmosphere was used as a reactor. A 10 g portion of OMMT and 0.07 g of toluene-p-sulfonic acid (catalyst, purity 99%, reagent grade, Shanghai Guoyao Chemical Company) were added slowly to 0.06 mol of the previously prepared solvent of N,N-dihydroxyl-3-aminomethyl propionate (see above). The resultant suspension was stirred vigorously for 10 h. The OMMT thus treated was washed with methanol three times until no viscous materials remained. The filter cake was then placed in a vacuum oven at 80ºC for 6 h for drying. The dried cake was ground to a particle size of <1 μm to obtain the intermediate compound, with a yield of ~90%.

In step 3 (Figure 1), 0.1 L of 1 mol/L of intermediate (purity 90%) and 0.1 L of 2 mol/L phosphate (H_3PO_4, purity 98%, reagent grade, Shanghai Lingfeng Chemical Company) were added to a three-necked flask with an integrated stirrer. The mixtures were treated at ~75−80ºC for ~2 h. The product was filtered and filter washed with acetone (purity 99%, reagent grade, Shanghai Lingfeng Chemical Company). The product, FR-HOMMT, was obtained and the yield was ~85%.

Preparation of NR/OMMT and NR/FR-HOMMT composites

In the last step, different additives were added into the NR systems on a double roller plasticator (Shanghai Second Rubber Machinery Factory, XK-1600, Shanghai, China). After mixing for 20 min, OMMT or FR-HOMMT was added, and NR/OMMT or NR/FR-HOMMT composites were produced. Then, the mixture was added to a dumbbell mould. Curing was conducted at 150ºC for 10 min, after which an elastic vulcanizate was obtained.

The formulation (Table 1) was used for the application of OMMT or the novel FR-HOMMT to rubber vulcanizates.

Characterization

The FTIR spectra of OMMT, intermediate, and FR-HOMMT were obtained using a Nicolet Avatar 370 FTIR spectrophotometer (Nicolet Instruments, Inc., Madison, Wisconsin, USA). The scanning range was from 4000 to 700 cm^{-1} with a resolution of 2 cm^{-1}. 1 mg of sample was ground and mixed with 100 mg of KBr to form pellets. Sixty-four scans were necessary to obtain spectra with good signal-to-noise ratios.

The XRD patterns of OMMT, intermediate, and FR-HOMMT were obtained by packing the air-dried, finely ground samples into an aluminum sample holder, and scanning from 1 to 10º2θ at a rate of 2º2θ/min. A Rigaku D-Max/400 X-ray diffractometer and goniometer (Tokyo, Japan) was used. The X-ray beam was Ni-filtered CuKα (λ = 0.154 nm) radiation operated at 50 kV. The corresponding basal (d_{001}) spacings were derived from the first-order reflections by applying Bragg's law.

Scanning electron microscopy of OMMT, the intermediate, FR-HOMMT, and the section morphology of different NR composites was carried out using an Hitachi S-2150 scanning electron microscope (electron beam potential of 25 kV; operating current of 50 μA). The specimens were previously coated with a conductive gold layer (Dong, 2004).

The thermogravimetric analysis (TGA) of OMMT, intermediate, FR-HOMMT, and the corresponding NR composites was carried out at 20ºC/min under nitrogen using a Linseis PT-1000 microbalance (Selb, Germany). In each case, the mass of sample used was 10 mg. The samples (powder mixtures) were positioned in open vitreous silica pans and examined at temperatures ranging from room temperature to 700ºC.

The curing parameters of the NR/OMMT and NR/FR-HOMMT composites were determined using an oscillating disk rheometer (MDR-2000, Wuxi, Liyuan, China) according to ASTM D 2084-81 (2011). The compositions were then vulcanized at 150ºC using the appropriate optimum cure time. The optimum cure time, t_{90}, one of the curing parameters, was tested by means of the oscillating disk rheometer under 15 MPa pressure on an electrically heated press. In order to compare test results most conveniently, all of the uncured mixes and vulcanizates in the present study were prepared using the conditions and formulation outlined above (Table 1).

The tensile properties of the vulcanizates were measured using the dumbbell specimens (6 mm wide

Table 1. Formulation of rubber vulcanizates.

Component	phr (parts per hundred of rubber)
NR	100
Sulfur	2.5
Zinc oxide	5.0
Stearic acid	1.0
2-bezothiazolethiol	1.2
Tetramethyl thiuram disulfide	0.2
Diphenyl guanidine	0.3
Antioxidant D	1.0
OMMT or FR-HOMMT	0, 5, 10, 15, 20

in cross section) according to the Chinese National Standard GB 528-82. The value for each sample was taken as the median value of five specimens. These tests were carried out at room temperature on a universal tensile testing machine (TCS-2000, Dongguan, China) with a crosshead speed of 500 mm/min. The tensile strength for specimens of each composition was tested, and the stress and strain at break were determined.

The wear-resistance tests of the vulcanized rubber composites were conducted using a WML-76 Akron abrasion testing machine (Jiangsu Zhenwei Company, Yangzhou, Jiangsu, China). The rotating velocities of the sample wheel and the emery wheel were 76 rpm and 33 rpm, respectively. The angle between the shafts of the two related wheels was 15°. A pressure of 26.7 N/m^2 was applied to the sample during the wearing process.

A Limiting Oxygen Index (LOI) was measured using a HC-2 instrument (Nanjing, China) on sheets (120 mm × 6 mm × 3 mm in size) according to ASTM 2863 (2011). The photographic images of the horizontal burning of these composites were captured using a Sony digital camera (Sony Cyber-shot DSC-W55/P, Sony Camera, New York, USA).

RESULTS AND DISCUSSION

Analysis of FR-HOMMT

FTIR. The FTIR spectra of OMMT, the intermediate, and FR-HOMMT (Figure 2a) revealed typical structural stretching vibrations at ~3630 cm^{-1} for OMMT. The water present in the silicate layers contributed to stretching vibrations with a broad band located at ~3435 cm^{-1}, and to deformation vibrations at ~1635 cm^{-1} (Shen *et al*., 2009). The deformation vibrations of structural -OH groups in OMMT depended on the chemical composition of material used, *e.g*. Al-Al-OH vibrations can be found at 920 cm^{-1}, Al-Fe-OH at 875 cm^{-1}, and Al-Mg-OH at 845 cm^{-1}. Complex bands at 1050 cm^{-1} were typical of stretching vibrations of Si−O and Al−O bonds in the OMMT structure. In addition, the peaks at 2880−3000 cm^{-1} and 1469 cm^{-1} were ascribed to the stretching and deformation vibration of C−H and attributed to the methyl or methylene groups which existed in the intercalation agent, N,N-di(2-hydroxyethyl)-N-dodecyl-N-methylammonium chloride.

For the intermediate, a broad peak at 3250−3650 cm^{-1} was evident, and caused by the introduction of more hydroxyl groups to OMMT by the hyper-branched technology. The peak at 1650 cm^{-1} resulted from −C=O and −C−O bonds in $-CH_2CH_2COOCH_3$, a linear unit in the hyper-branched macromolecular chain. In addition, the peak at 1250 cm^{-1} was probably assigned to the stretching vibration of the C−N bond and was due to the addition reaction between methyl acrylate and diethanolamine (Figure 1b) belonging to the Michael addition reaction. The H atom of −NH− in diethanolamine was very reactive and was able to react with −C=C− in methyl acrylate to produce  . The methanol used here was a kind of solvent and phase-transfer agent. It could accelerate dissolution of the two reactants and improve their reaction rate.

In the FR-HOMMT spectrum, new peaks at 1650 and 1050 cm^{-1} were evident, resulting from corresponding stretching and deformation absorptions in the final product. The appearance of peaks at 1650 and

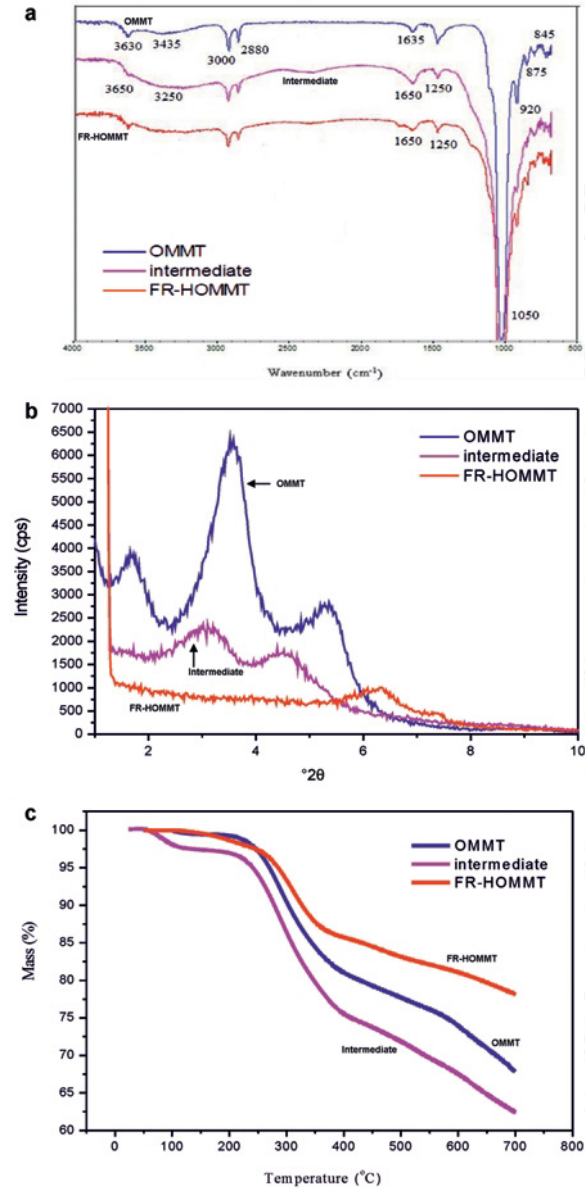

Figure 2. Characterization of OMMT, intermediate, and FR-HOMMT by: (a) FTIR; (b) XRD, and (c) TGA.

1050 cm^{-1} was attributed to the P=O and P−O bonds in $-POOCH_2CH_3$, the branched unit in the hyper-branched macromolecules. These groups came from the esterification reaction between phosphate and hydroxyl in the intermediate (Ma *et al*., 2003; Dai *et al*., 2008).

XRD

The XRD spectra of OMMT, the intermediate, and FR-HOMMT (Figure 2b) revealed that the basal spacing (d_{001}) of the organo-clays varied between 1.2 and 4.9 nm; some had been exfoliated and the interlayer spacing could not be calculated.

In curve a, three peaks were shown at 1.8º, 3.5º, and 5.4º2θ and ascribed to the different degrees of expansion of silicate layers in the OMMT. The appreciably larger basal spacing (4.9 nm) for the quaternary ammonium ion-treated samples, compared with the other organo-clays, might be due to the paraffin-type arrangement or interlayer entry of ammonium hydrolysis products during synthesis.

The shifting of peaks from 3.5 and 5.4º2θ to 3.2 and 4.6º2θ, as shown in curve b, indicated the increasing interlayer spacing caused by the hyper-branched technology. The basal spacings of 1.9 to 2.7 nm for the intermediate were consistent with bilayer to pseudo-trilayer arrangement of the intercalated surfactants.

As observed in curve c, the shifting of peaks to 6.2 and 7.4º2θ illustrated the decreasing interlayer spacing. The calculated values of 1.2 to 1.4 nm for FR-HOMMT were consistent with a monolayer arrangement of the P in the hyper-branched polymer in the interlayer space. Moreover, the disappearance of peaks at 1.8, 3.2, and 4.6º2θ might be ascribed to the development of exfoliated silicate layers in the modified powders (Churchman *et al.*, 2006; Ruiz-Hitzky and Van Meerbeek, 2006). The intercalation or exfoliation may have been caused by the energy produced by condensation and esterification reactions between OMMT, the monomer, and phosphate (Fang *et al*., 2009; Hu *et al*., 2006; Wang *et al*., 2009b).

TGA

The TGA curves for OMMT, the intermediate, and FR-HOMMT (Figure 2c) revealed that the weight loss of OMMT in the curves near 100ºC may be ascribed to the evolution of absorbed water and gaseous species. A downward shift of similar magnitude was also reported by He *et al.* (2005) for montmorillonite modified with hexadecyltrimethyl ammonium ions. Weight loss by the organo-clay between 220 and 700ºC was ascribed to dehydroxylation of the montmorillonite. Xie *et al.* (2001, 2002) suggested 700ºC as the upper limit for dehydroxylation of the clay, while Xi *et al.* (2005) preferred 636ºC as the limit.

After modification by hyper-branched polymers, the weight loss of the intermediate in the low-temperature range occurred at ~50ºC, a change from that of OMMT. These observations might be explained in terms of the hydrophobic nature of the hyper-branched polymer. As the residual water molecules in the organo-clay are contained in the spaces ('pores') between the interlayer quaternary ammonium ions, rather than being directly associated with the hyper-branched polymer, they are relatively weakly held (Lagaly *et al.*, 2006).

In discussing the thermal characteristics of some phosphonium-modified clay, Xie *et al.* (2002) separated the curves into four distinct regions: (I) evolution of free water and gases below 150ºC; (II) evolution of organic substances between 150 and 550ºC; (III) dehydroxylation of the montmorillonite between 550 and 700ºC; and (IV) evolution of carbonaceous residues after temperature became >700ºC. The thermal behavior of the organo-clays in region II was very important in terms of their function as flame-retardant agents for NR because the interlayer surfactants began to decompose in this temperature range. The FR-HOMMT clearly had an enhanced thermal stability in this temperature range in comparison with that of OMMT, a benefit of the application of organo-clay to polymeric materials (Wang *et al*., 2009c).

Analysis of NR/FR-HOMMT composites

Cure characteristics. The cure characteristics data for different amounts and types of OMMT-filled NR systems are shown (Figure 3). The scorch time, t_{10}, describes the time during which a rubber compound can be worked safely at a given temperature before curing begins in rubber manufacture. The optimum cure time, t_{90}, is the time taken for the rubber to rise to its maximum point of crosslinking density, and at 90% of this level.

The scorch time (t_{10}) was increased with increasing filler loading for OMMT- and FR-HOMMT-filled NR vulcanizates. However, the addition of FR-HOMMT could decrease scorch time, thus making processing a

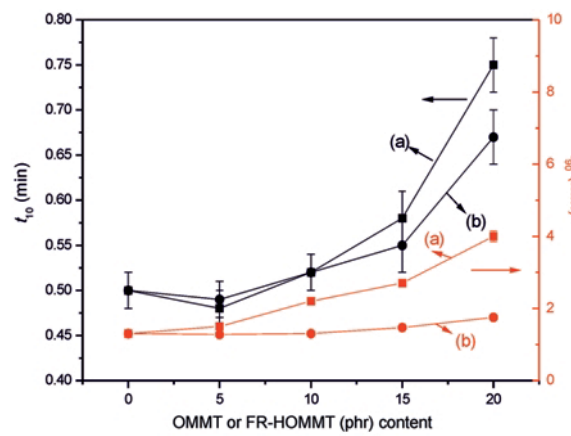

Figure 3. t_{10} (black traces) and t_{90} (gray traces) of (a) NR/OMMT, and (b) NR/FR-HOMMT.

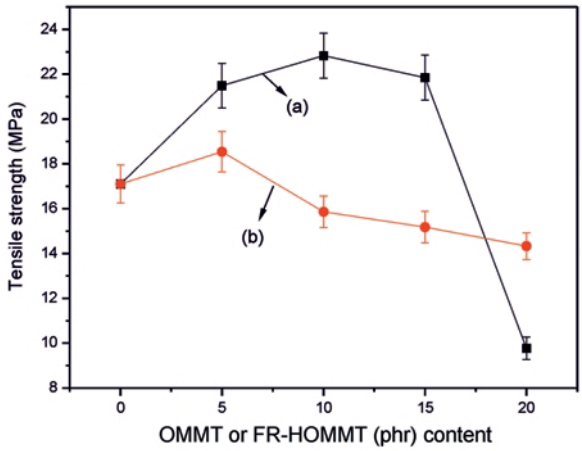

Figure 4. Tensile strengths of (a) NR/OMMT, and (b) NR/FR-HOMMT.

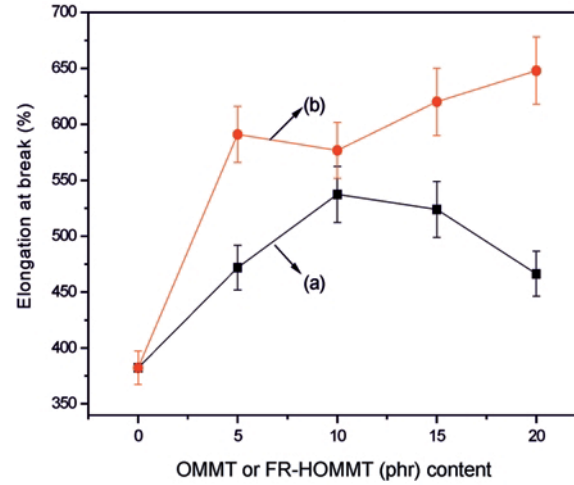

Figure 5. Elongation at break of (a) NR/OMMT, and (b) NR/FR-HOMMT.

little unsafe compared with that of OMMT-filled systems. The decreased scorch time for the NR/FR-HOMMT system was attributed to the adsorption of a curative, the sulfate agent, by the hyper-branched polymers (Ramesan, 2005).

The optimum cure time (t_{90}) had almost the same trend as the scorch time. Energy was saved using the shortened optimum cure time in the vulcanization process.

Tensile properties

The composite based on 20 phr of FR-HOMMT showed a tensile strength value and an elongation-at-break value of up to 14.33 MPa and 650%, respectively, compared with values of 9.77 MPa and 460% for 20 phr of an OMMT-filled matrix (Figures 4, 5).

The complex interplay between the hyper-branched polymer and the induced increase in the apparent degree of cross-linking was the reason for such an increase (Labruyèrè, *et al.*, 2009). Other than for 20 phr of FR-HOMMT-reinforced matrix, the tensile strength of most NR/FR-HOMMT composites was less than comparative values for NR/OMMT composites. In addition, other than for the 5 phr of OMMT-reinforced matrix, all other values were smaller than those of unfilled NR because the tensile strength was very sensitive to the degree of clay dispersion in the polymer matrix. Small clay stacks were probably responsible for the smaller values (Liu *et al.*, 2003; Yoon *et al.*, 2007).

The failure of the two specimens started with small cracks generated by different types of holes. If the elastomeric network were capable of dissipating the input energy (*e.g.* by converting it to heat), then it would be able to withstand greater stress. The different crack characteristics of NR/OMMT-20 phr and NR/FR-HOMMT-20 phr under tension are depicted (Figure 6).

In NR/OMMT-20 phr, large cracks were generated by numerous aggregated OMMT, and this led to lower

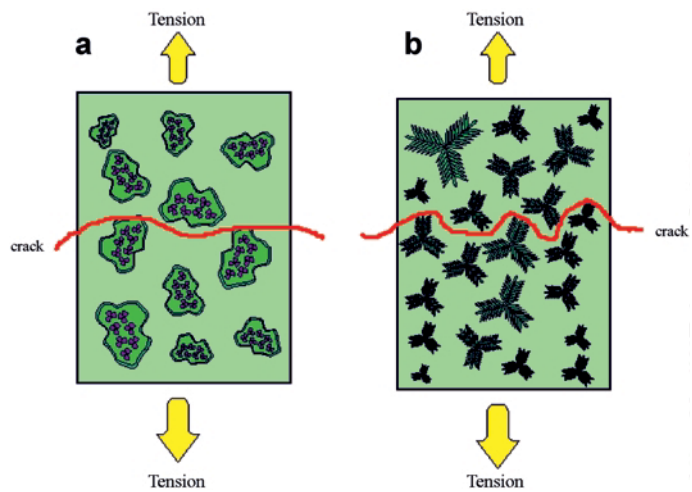

Figure 6. Reinforcing mechanism of (a) NR/OMMT-20 phr, (b) NR/FR-HOMMT-20 phr (phr = parts per hundred of rubber).

tensile strength. The fracture mechanism of NR/FR-HOMMT-20 phr was assumed to be chain slippage and 'zig-zag' energy dissipation. The hyper-branched polymer organic silicate layers dispersed uniformly in the polymeric matrix. The 'anchor' effect between the hyper-branched polymer and molecular chains in NR could restrict the movement of polymer chains and combine them with OMMT. The increase in the crack path around the silicate layers ('zig-zag' route, Figure 6b) may also be considered as a mechanism of energy dissipation. By this suggested model, the increase in tensile properties seemed to be as expected for this reinforced composite (Gatos *et al*., 2004).

Typical SEM images of the microscopic morphology of NR/OMMT-20 phr and NR/FR-HOMMT-20 phr, together with the corresponding OMMT and FR-HOMMT, confirm the hypothesis above.

Original OMMT layers were dispersed irregularly on the surface of the NR matrix and formed agglomerates (Figure 7a). In addition, due to poor compatibility, some silicate layers were pulled off by the applied tension. The fractured section of the NR was replete with deep cavities generated by the tension. On the other hand, in the NR/FR-HOMMT system, the number of cavities was zero (Figure 7b), and the novel hyper-branched silicate layers were dispersed almost uniformly. These results

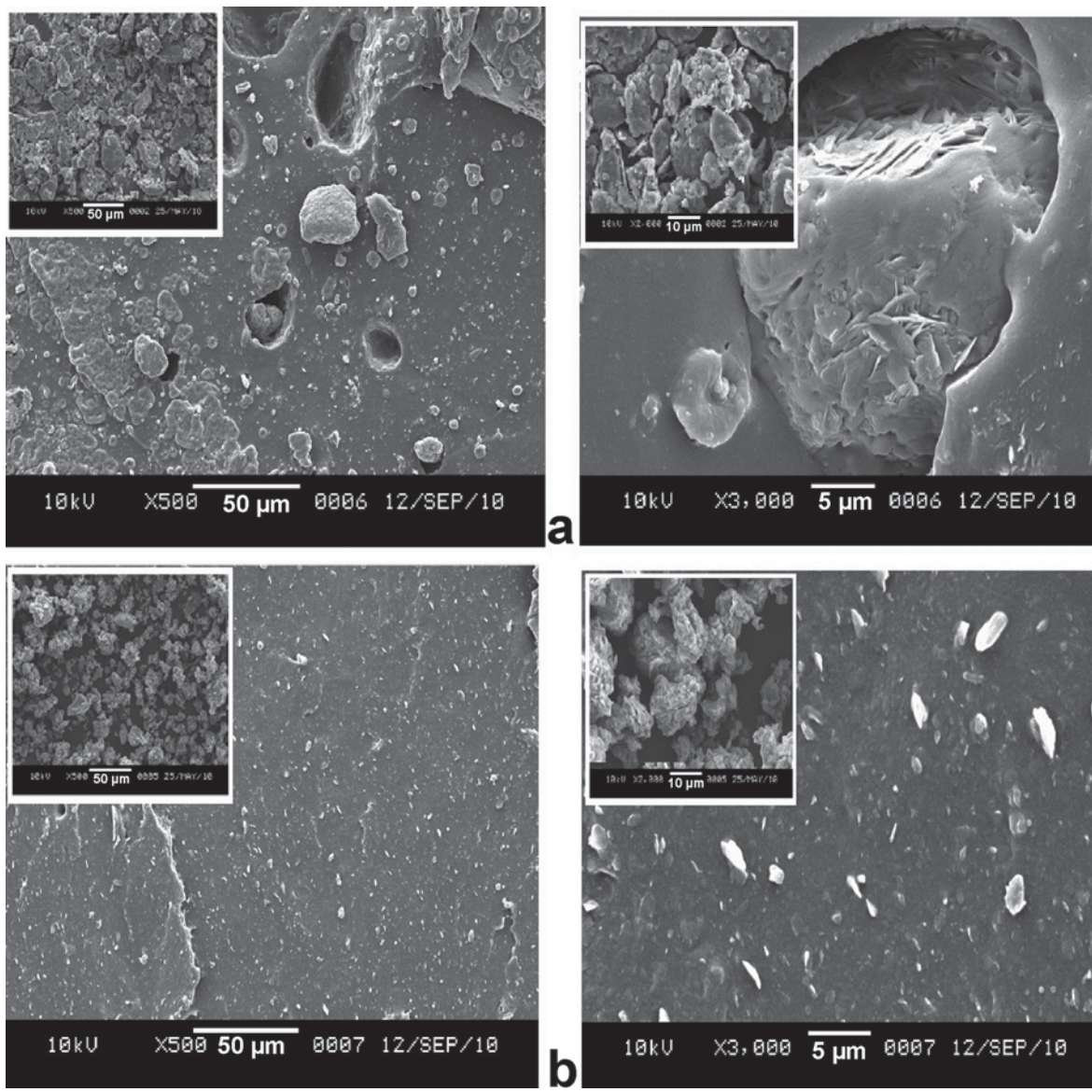

Figure 7. SEM images of section morphology of (a) NR/OMMT-20 phr, and (b) NR/FR-HOMMT-20 phr (phr = parts per hundred of rubber).

were in good agreement with the morphology and structure of original OMMT and FR-HOMMT powders.

Analysis by SEM of OMMT and FR-HOMMT powders is challenging, *e.g.* in terms of sample preparation, selection of particles, choice of crystal face, colloidal properties, *etc*., perhaps reflecting the structures of these clays (Zhu *et al.*, 2009).

The major difference in the morphology and surface structure between the two samples was that the surface roughness of montmorillonite decreased after modification by the hyper-branched polymer (Figure 7). This decrease was consistent with the trend of the fractal dimension determined by this scanning method. The OMMT consisted of powders, the particle size of which was ~50 μm (Figure 7a). Polymeric materials covered the surface of OMMT, and many small silicate layers were embedded in the larger layers (Figure 7b). In addition, the silicate layers were easily separated, indicating that the hyper-branched technology was beneficial in the dispersion of aggregated powders (Wang *et al*., 2009b).

Wear-resistance properties

Wear resistance is thought to affect not only the performance, but also the life expectancy of rubber products. The abrasion loss (the volume loss due to the abrasive action of rubbing a test piece over a specified grade of abrasive sheet) of the NR composites changed significantly with the addition of hyper-branched polymer-modified organo-clays.

In the present study, the abrasion consisted of micro-cutting by sanding the soft rubber surface of the composite under the grinding wheel of an Akron grinding machine in accordance with the line abrasion mechanism proposed by Burwell (1957). First, a crack was initiated in the surface of the rubber when the shearing force produced by the friction exceeded the limited shear strength of the rubber. Secondly, a tongue-shaped piece material appeared after the initiation of crack. Thirdly, the tongue-shaped piece of material ruptured and broke off the rubber matrix during the periodical friction, and thus the ridge-like morphology was developed.

The abrasion losses with different fillers are shown and compared (Figure 8). The abrasion loss was greater for NR with increasing amounts of OMMT than for NR with increasing amounts of FR-HOMMT (Figure 8a). The abrasion loss of the composite NR/OMMT-20 phr was 1.008 cm^3, ~481% greater than for unmodified NR. Due to the greater compatibility between NR and the silicate layers of the hyper-branched polymers, the system showed better wear resistance after the addition of FR-HOMMT (Figure 8b). The abrasion loss of the NR/FR-HOMMT-20 phr was 0.420 cm^3; the equivalent value for the NR/OMMT-20 phr composite was 1.008 cm^3.

Flame-retardance performance

The Limiting Oxygen Index (LOI) value of pure NR was small (16.0%, Figure 9), meaning that the NR was easily flammable (see the horizontal burning test in Figure 10). By adding 5−20 phr of OMMT to pure NR, the LOI value increased to 25.5%. The NR/OMMT-10 phr composite could also be ignited (Figure 10b), and the amount of residual char was smaller. With the addition of FR-HOMMT to NR systems, the LOI value increased to 31.0% (see the horizontal burning of the NR/FR-HOMMT-10 phr composite, Figure 10c). The fire in this case was very small, and the char layer was thicker than that of NR/OMMT-10 phr. These composites showed better fire protection than unomodified NR, probably due to the flame-retardant effect of the OMMT and phosphate. At least some of the improvement in flame-retardance for NR/FR-HOMMT composites can be explained by the formation of carbonaceous layers

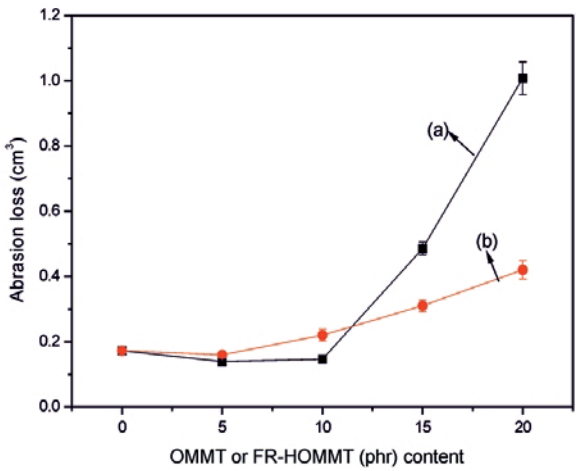

Figure 8. Abrasion loss of (a) NR/OMMT, and (b) NR/FR-HOMMT.

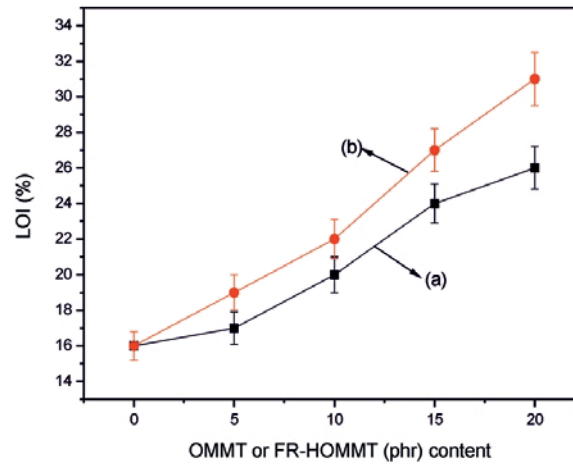

Figure 9. Limiting oxygen index (LOI) (a) NR/OMMT, and (b) NR/FR-HOMMT.

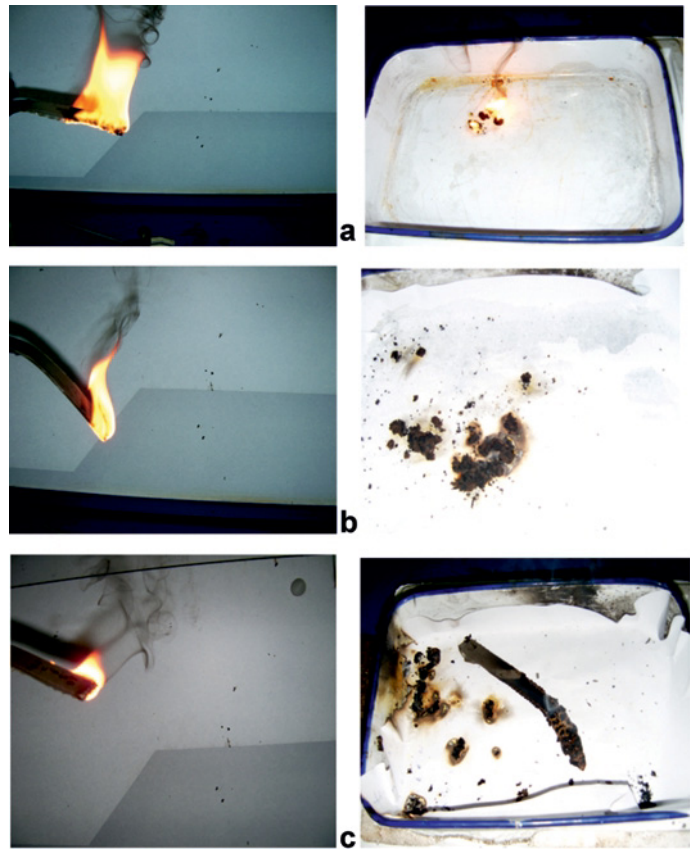

Figure 10. Burning of (a) NR, (b) NR/OMMT-10 phr, and (c) NR/FR-HOMMT-10 phr.

during burning which had a great effect on this property (Figure 11). The fire-retardancy properties of NR-FR-HOMMT might be explained as follows: first, the macromolecules of NR decomposed at high temperatures, and aromatic compounds were developed from the phosphorus ester in the hyper-branched polymer. Secondly, carbonaceous layers were produced from these aromatic compounds, and better fire-retardance properties were obtained for these composites. Thirdly, the silicate layers of OMMT inhibited and restricted the degree of pyrolysis of the NR matrix. They were able to act as a physical barrier and prevent combustible gases from feeding the flame, and also to keep oxygen separate from the burning material (Li *et al*., 2009).

Thermal stability

In an attempt to further elucidate the flame-retardant effect of phosphorus and silicone elements, the thermal behavior of NR, NR/OMMT-10 phr, and NR/FR-HOMMT-10 phr composites was analyzed by TGA.

In order to compare their thermal stabilities, four parameters were measured from the TGA curves, *i.e.* the onset temperature of thermal degradation (T_{onset}, the temperature at which weight loss = 5 wt.%), the middle

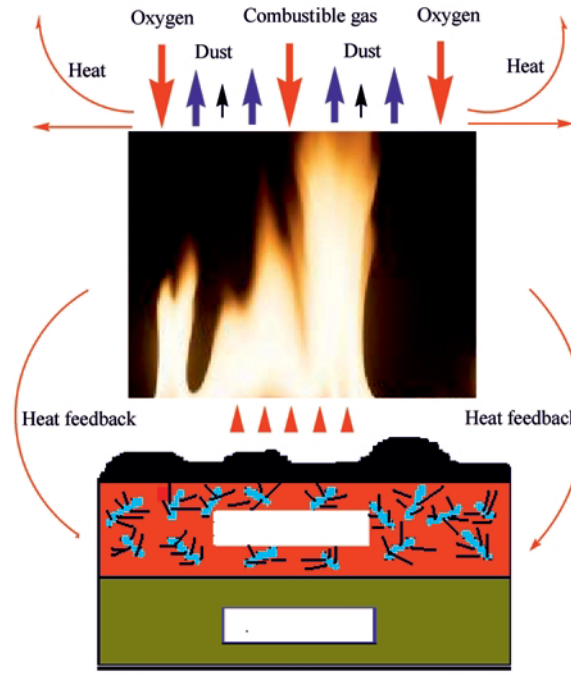

Figure 11. Flame-retardant mechanism for FR-HOMMT in NR.

Table 2. TGA results for the thermal degradation of different NR systems.

Sample	T_{onset} (ºC)	$T_{0.5}$ (ºC)	T_f (ºC)	Charred residue at 700ºC (wt.%)
NR	303	390	598	8.97
NR/OMMT-10 phr	309	400	657	13.30
NR/FR-HOMMT-10 phr	323	401	688	15.59

phr: parts per hundred of rubber

temperature ($T_{0.5}$, the temperature at which weight loss = 50 wt.%), the terminal temperature of thermal degradation (T_f, the temperature after which no significant weight loss was observed), and the yield of charred residue at 700ºC (results in Table 2).

The T_{onset}, $T_{0.5}$, and T_f increased by 6, 10, and 59ºC, respectively, when 10 phr of OMMT was added to NR (Figure 12, traces a,b). Moreover, the residual weight at 700ºC was improved by ~4.33 wt.% indicating that the OMMT did have some flame-retardant effect and formed a barrier layer hindering the diffusion of gases to increase the temperature of degradation. However, OMMT alone could not effectively enhance the flame retardance of NR. Unlike the NR/OMMT system, significant improvement of T_{onset} and T_f was obtained when 10 phr of FR-HOMMT was added to NR.

The results above were in accordance with the LOI results and confirmed the fact that the phosphorus in the hyper-branched polymer and the silicone element in the OMMT had a flame-retardant effect, thereby enhancing the thermal stability of NR (Hassan *et al*., 2007; Xia *et al*., 2007).

CONCLUSIONS

OMMT is an effective filler for improving the mechanical and flame-retardance properties of NR composites. Surface modification by an appropriate amount of hyper-branched polymer and phosphate improved the tensile-strength and flame-retardant properties for the NR matrix. Experimental results demonstrated that incorporation of 20 phr of FR-HOMMT into NR increased the tensile strength from 9.77 to 14.33 MPa and elongation at break from 460 to 650% compared with that of 20 phr OMMT-filled composites. Meanwhile, the abrasion loss of NR/FR-HOMMT-20 phr was 0.420 cm^3, 140% less than that of the NR/OMMT-20 phr composite, 1.008 cm^3. With the addition of FR-HOMMT to NR systems, the LOI value increased to 31.0%, and the thermal stability was also improved.

A mechanism for reinforcing the flame-retardant ability of FR-HOMMT was proposed. Modification of OMMT powder by hyper-branched polymer would improve the compatibility between the filler and the NR matrix. As a result, this addition might increase the crack propagation path and improve the tensile properties for NR composites. Carbonaceous layers developed from hyper-branched polymer and silicate layers could inhibit the degree of pyrolysis of the rubber systems, and thus improve the flame-retardant properties for the NR matrix.

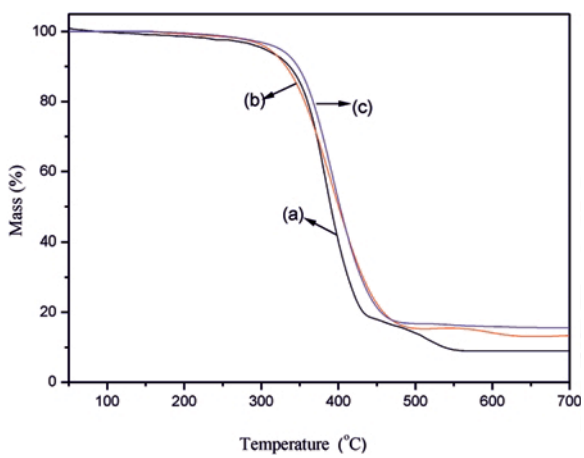

Figure 12. TGA of (a) NR, (b) NR/OMMT-10 phr, and (c) NR/FR-HOMMT-10 phr.

ACKNOWLEDGMENTS

This work was supported financially by the National Natural Science Funds (Project No.50803034 and No, 51173102), by the Shu Guang project (No. 10SG53) supported by Shanghai Municipal Education Commission and Shanghai Education Development Foundation, by Shanghai Nano-project Funds (Project No. 0952nm02600), and by Shanghai Universities Knowledge Innovation Engineering Project (Project No. JZ0904).

REFERENCES

Aouad, A., Anastácio, A.S., Bergaya, F., and Stucki, J.W. (2010) A Mössbauer spectroscopic study of aluminum- and iron-pillared clay minerals. *Clays and Clay Minerals*, **58**, 164−173.

ASTM D2084-81 (2011) Standard test method for rubber property-vulcanization using oscillating disk cure meter. American Society for Testing and Materials.

ASTM D2863-10 (2011) Standard test method for measuring the minimum oxygen concentration to support candle-like combustion of plastics (oxygen index). American Society for Testing and Materials.

Boo, W.J., Liu, J., and Sue, H.J. (2006) Fracture behavior of nanoplatelet reinforced polymer nanocomposites. *Material Science and Technology*, **22**, 829−834.

Burwell, J.T. (1957) Survey of possible wear mechanism. *Wear*, **1**, 119−123.

Calderon, J.U., Lennox, B., and Kamal, M.R. (2008) Thermally stable phosphonium-montmorillonite organo-clays. *Applied Clay Science*, **40**, 90−98.

Churchman, G.J., Gates, W.P., Theng, B.K.G., and Yuan, G. (2006) Clays and clay minerals for pollution control. Pp. 625−675 in: *Handbook of Clay Science* (F. Bergaya, B.K.G. Theng, and G. Lagaly, editors). Elsevier, Amsterdam.

Dai, C.F., Li, P.R., and Yeh, J.M. (2008) Comparative studies for the effect of intercalating agent on the physical properties of epoxy resin-clay based nanocomposite materials. *European Polymer Journal*, **44**, 2439−2447.

Dong, Y.M. (2004) *Polymer Analysis Handbook*. China Petrochemical Press, Beijing, pp. 521−522.

Fang, S.L., Hu, Y., Song, L., and Wu, J. (2009) Preparation and investigation of ethylene-vinyl acetate copolymer/silicone rubber/clay nanocomposites. *Journal of Applied Polymer Science*, **113**, 1664−1670.

Gatos, K.G., Sawanis, N., Apostolov, A.A.,Thomann, R., and Karger-Kocsis, J. (2004) Nanocomposite formation in hydrogenated nitrile rubber (HNBR)/organo-montmorillonite as a function of intercalant type. *Macromolecular Materials and Engineering*, **289**, 1079−1086.

Gu, Z., Song, G.J., Liu, W.S., Yang, S.J., and Gao, J.M. (2010) Structure and properties of hydrogenated nitrile rubber/organo-montmorillonite nanocomposites. *Clays and Clay Minerals*, **58**, 72−78.

Hassan, M.A., Kozlowski, R., Obidzinski, B., Shehata, A.B., and Aziz, F.A. (2007) The effect of new flame retardant systems containing montmorillonite-butyl acrylate nanoclay on the flammability properties of polyuerethane polymer. *Polymer-Plastics Technology and Engineering*, **46**, 521−527.

He, H., Ding, Z., Zhu, J., Yuan, P., Xi, Y., Yang, D., and Frost, R.L. (2005) Thermal characterization of surfactant-modified montmorillonite. *Clay and Clay Minerals*, **53**, 287−293.

Hedley, C.B., Yuan, G., and Theng, B.K.G. (2007) Thermal analysis of montmorillonites modified with quaternary phosphonium and ammonium surfactants. *Applied Clay Science*, **35**, 180−188.

Hu, Y., Tang, Y., and Song, L. (2006) Poly(propylene)/clay nanocomposites and their application in flame retardancy. *Polymers for Advanced Technologies*, **17**, 235−245.

Ismail, H., Munusamy, Y., Mariatti, M., and Ratnam, C.T. (2008) Preparation and characterization of EVA/SMRL/organo-clay nanocomposites: effect of blending sequences and organo-clay loading. *Polymer-Plastics Technology and Engineering*, **47**, 752−761.

Labruyèrè, C., Monteverde, F., Alexandre, M., and Dubois, P. (2009) Exfoliation of clays in poly(dimethylsiloxane) rubber using an unexpected couple: a silicone surfactant and water. *Journal of Nanoscience and Nanotechnology*, **9**, 2731−2738.

Lagaly, G., Ogawa, M., and Dekany, I. (2006) Clay mineral-organic interactions. Pp. 309−377 in: *Handbook of Clay Science* (F. Bergaya, B.K.G. Theng, and G. Lagaly, editors). Elsevier, Amsterdam.

Lee, S.Y., Cho, W.J., Kim, K.J., Ahn, J.H., and Lee, M. (2005) Interaction between cationic surfactants and montmorillonite under non-equilibrium conditions. *Journal of Colloid and Interface Science*, **284**, 667−673.

Li, B., Jia, H., Guan, L.M., Bing, B.C., and Dai, J.F. (2009) A novel intumescent flame-retardant system for flame-retarded LLDPE/EVA composites. *Journal of Applied Polymer Science*, **114**, 3626−3635.

Liu, T.X., Lim, K.P., Tjiu, W.C., Pramoda, K.P., and Chen, Z.K. (2003) Preparation and characterization of nylon 11/organo-clay nanocomposites. *Polymer*, **44**, 3529−3535.

Ma, J., Xu, J., Ren, J.H., Yu, Z.Z., and Mai, Y.W. (2003) A new approach to polymer/montmorillonite nanocomposites. *Polymer*, **44**, 4619−4624.

Marlene, R., Christopher, J.G.P., Laszlo, G., Yves, L., Henri, J.M.G., and Jan-Anders, E.M. (2004) Hyperbranched polymer/montmorillonite clay nanocomposites. *Polymer*, **45**, 949−960.

Menon, A.R.R. (1997) Flame-retardant characteristics of natural rubber modified with a bromo derivative of phosphorylated cashew nut shell liquid. *Journal of Fire Sciences*, **15**, 3−13.

Monasterio, F.E., Dias, M.L., Pita, V.J.R.R., Erdmann, E., and Destéfanis, H.A. (2010) Effect of the organic groups of difunctional silanes on the preparation of coated clays for olefin polymer modification. *Clay Minerals*, **45**, 489−502.

Powell, C.E. and Beall, G.W. (2007) Physical properties of polymer/clay nanocomposites. Pp. pp 561−575 in: *Physical Properties of Polymers Handbook*. Springer, Berlin.

Ramesan, M.T. (2005) The effects of filler content on cure and mechanical properties of dichlorocarbene modified styrene butadiene rubber/carbon black composites. *Journal of Polymer Research*, **11**, 333−340.

Ruiz-Hitzky, E. and Van Meerbeek, A. (2006) Clay minerals and organoclay-polymer nanocomposites. Pp. 583−621 in: *Handbook of Clay Science* (F. Bergaya, B.K.G. Theng, and G. Lagaly, editors). Elsevier, Amsterdam.

Shen, W., He, H.P., Zhu, J.X., Yuan, P., Ma, Y.H., and Liang, X.L. (2009) Preparation and characterization of 3-aminopropyltriethoxysilane grafted montmorillonite and acid-activated montmorillonite. *Chinese Science Bulletin*, **54**, 265−271.

Tan, H.M. and Luo, Y.J. (2005) *Hyper-branched Polymers*, Chemical Industry Press, Beijing.

Wang, J.C. and Chen, Y.H. (2007) Synthesis of an intumescent flame retardant (IFR) agent and application in a natural rubber (NR) system. *Journal of Elastomers and Plastics*, **39**, 33−51.

Wang, J.C., Chen, Y.H., and Jin, Q.Q. (2006) Preparation and characteristics of a novel silicone rubber nanocomposite based on organophilic montmorillonite. *High Performance Polymers*, **18**, 325−340.

Wang, J.C., Chen, Y.H., Jin, Q.Q., Tang, Y., and Xu, M.M. (2009a) Preparation, properties, and mechanism of novel polyurethane adhesive/organic montmorillonite nanocomposites. *High Performance Polymers*, **21**, 155−171.

Wang, J.C., Chen, Y.H., and Wang, J.H. (2009b) Synthesis of hyperbranched organo-montmorillonite and its application into high-temperature vulcanizated silicone rubber systems. *Journal of Applied Polymer Science*, **111**, 658−667.

Wang, J.C., Yang, K., and Zheng, X.Y. (2009c) Preparation and characterization of hyper-branched and nano-type organo-montmorillonite silicate layers. *Proceedings of 2009 International Conference on Advanced Fibers and Polymer Materials*, Volume II, 1019−1022.

Xi, Y., Martens, W., He, H., and Frost, R.L. (2005) Thermogravimetric analysis of organo-clays intercalated with the surfactant octadecyltrimethylammonium bromide. *Journal of Thermal Analysis and Calorimetry*, **81**, 91−97.

Xia, Y., Jian, X.G., Li, J.F., Wang, X.H., and Xu, Y.Y. (2007) Synergistic effect of montmorillonite and intumescent flame retardant on flame retardance enhancement of ABS. *Polymer-Plastics Technology and Engineering*, **46**, 227−232.

Xie, W., Gao, Z., Pan, W.P., Hunter, D., Singh, A., and Vaia, R. (2001) Thermal degradation chemistry of alkyl quaternary ammonium montmorillonite. *Chemistry of Materials*, **13**, 2979−2990.

Xie, W., Xie, R., Pan, W.P., Hunter, D., Koene, B., Tan, L.S., and Vaia, R. (2002) Thermal stability of quaternary

phosphonium modified montmorillonite. *Chemistry of Materials*, **14**, 4837–4845.

Xu, B., Zheng, Q., Song, Y.H., and Shangguan, Y. (2006) Calculating barrier properties of polymer/clay nanocomposites: effect of clay layers. *Polymer*, **47**, 2904–2910.

Yoon, K.B., Sung, H.D., Hwang, Y.Y., Noh, S.K., and Lee, D.H. (2007) Modification of montmorillonite with oligomeric amine derivatives for polymer nanocomposite preparation. *Applied Clay Science*, **38**, 1–8.

Zhao, F., Bao, X.J., Andrew, R.M., Gu, J.J., Wan, C.Y., and Bala, K. (2010) Effect of POSS on morphology and mechanical properties of polyamide 12/montmorillonite nanocomposites. *Applied Clay Science*, **47**, 249–256.

Zhou, N.L., Xia, X.X., and Wang, Y.R. (2002) Study on mechanical property of exfoliated silicone rubber/clay nanocomposites. *Acta Polymerica Sinica*, **2**, 253–256.

Zhu, J.X., Zhu, L.Z., Zhu, R.L., Tian, S.L., and Li, J.W. (2009) Surface microtopography of surfactant modified montmorillonite. *Applied Clay Science*, **45**, 70–75.

(*Received 17 September 2010; revised 25 October 2011; Ms. 497; A.E. H. Dong*)